Available online at www.sciencedirect.com

ScienceDirect

journal homepage: www.elsevier.com/locate/he

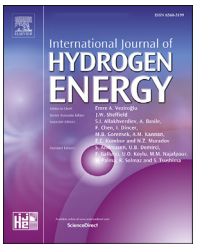

Numerical simulation of flame acceleration and deflagration-to-detonation transition in ammonia-hydrogen–oxygen mixtures

Ruixuan Zhu, Majie Zhao, Huangwei Zhang *

Department of Mechanical Engineering, National University of Singapore, 9 Engineering Drive 1, Singapore, 117576, Republic of Singapore

HIGHLIGHTS

- Numerical simulation of flame acceleration and transition to detonation are performed.
- Detailed chemistry of ammonia and hydrogen oxidation are used.
- For high ammonia content, hot spot triggers the DDT before the flame front.
- For high hydrogen content, local explosion occurs along the flame front for DDT.

ARTICLE INFO

Article history:
Received 30 December 2019
Received in revised form
22 September 2020
Accepted 27 September 2020
Available online xxx

Keywords:
DDT
Ammonia
Hydrogen
Detailed chemistry
Hot spot
Obstructed channel

ABSTRACT

Flame propagation and Deflagration-to-Detonation Transition (DDT) in a two-dimensional obstructed channel filled with stoichiometric ammonia-hydrogen-oxygen mixtures are simulated with detailed chemistry. For mixtures of high ammonia molar ratio ($\alpha = 4{:}1$ and 2:1), a hot spot with high temperature appears in the unreacted material, and then DDT is triggered by the reactivity gradient inside a pocket of unreacted material for $\alpha = 2{:}1$. However, for $\alpha = 4{:}1$, detonative initiation and failure alternatively occur. For mixtures with low ammonia ratios, the DDT is triggered when the flame interacts with the reflected shock waves from either the bottom wall or the obstacle. Furthermore, as the concentration of ammonia decreases, the flame acceleration, the appearance of noticeable shocks and the deflagration-to-detonation transition occur at an earlier instant, and the ultimate propagation velocities of detonation wave increase. The flame cannot propagate stably in premixed ammonia-oxygen mixture without hydrogen with the ignition mode adopted in this study.

Introduction

Hydrogen (H_2) has attracted lots of research interests in recent years since its combustion only generates water as the product. However, a series of technical challenges still exist when it is used as a fuel, including transport, storage and safety, which hinder the wide engineering applications of hydrogen energy. As an alternative fuel, ammonia (NH_3) is easily storable with high hydrogen content (approximately 17.7% w.t.), with lower storage cost of 0.54 $/kg-H, compared to 14.95 $/kg

* *Corresponding author.*
E-mail address: huangwei.zhang@nus.edu.sg (H. Zhang).

https://doi.org/10.1016/j.ijhydene.2020.09.227
0360-3199/

H for pure hydrogen storage [1]. Ammonia has already been produced and transported in considerable volumes (~180 Mtonnes/year [2]), and therefore potentially can be used as a fuel with sufficient supply. Furthermore, ammonia combustion does not generate carbon-related pollutant species. Therefore, novel techniques utilizing ammonia as a fuel can realize the carbon-free energy conversion process.

Hydrogen has wide flammability limit and low ignition energy, a hydrogen cloud could be easily ignited once leakage occurs, generating a slow or fast deflagration, or even a detonation [3]. Therefore the study on the deflagration and detonation properties of hydrogen-oxygen blends have triggered great research interests. Hydrogen has the fastest flame speed among practical fuels, and some experiments and numerical simulations indicate that the ignition and combustion performances of the natural gas (methane)-fueled engines could be greatly enhanced with the addition of hydrogen [4–8]. Hydrogen has also been characterized to be a superior addition for improving the combustion performance of hydrocarbon fuels, such as propane, methane and Liquefied Petroleum Gas (LPG) [9–12]. Detonation limits refer to the conditions outside of which a self-sustained detonation wave can no longer propagate [13,14], while near the limits, the propagation phenomenon of some hydrogen-oxygen blends is unsteady and more complex, including stable detonation, stuttering mode, galloping mode, and fast flame [15]. Large velocity fluctuations have been observed in hydrogen-air, hydrogen–oxygen and hydrogen–oxygen-diluent mixtures and in the detonable stoichiometric mixtures of hydrocarbons (C_2H_2, C_2H_4, C_2H_6, C_3H_8) with O_2, air or N_2O as the limits were approached [16,17]. Thus the dilution of hydrogen-oxygen mixtures with ammonia plays an important role in the steady propagation of detonative combustion.

Nevertheless, there are still some issues for ammonia combustion, e.g. slow chemical kinetics of ammonia oxidation and therefore slow burning velocity, high ignition energy, narrow flammability range and also poor flame stabilization characteristics. To tackle these problems, numerous experimental and numerical simulations have been performed. For example, the combustion characteristics of premixed ammonia-air mixtures at elevated pressure and temperature conditions (1–49 atm, 298–732 K) during the spark-ignition engine operation were simulated numerically and laminar burning velocity peaked at ammonia–air equivalence ratio (φ) of 1.12, while the adiabatic flame temperature peaked at stoichiometric condition. (φ = 1.01) [18]. Moreover, experimental and numerical studies were performed to determine the combustion and emission features of ammonia–methane blends using swirling flows representative of gas turbines [19].

Ammonia-addition into hydrogen could overcome some drawbacks in pure hydrogen and pure ammonia fuel and has been extensively extended in the internal combustion engine and gas turbine [20,21]. Ichikawa found that the laminar burning velocity of ammonia/air mixture increases non-monotonically with hydrogen substitution, and that Markstein length changes non-monotonically with hydrogen addition [22]. Lee [23] pointed out that NO_x and N_2O formation could be enhanced by ammonia substitution on hydrogen/air flame, and the amount of NO_x emissions on rich side increases and then decreases with ammonia substitution. The explosion hazard of hydrogen/ammonia fuel was evaluated by Li to establish safety precautions and ensure energy utilization [24]. The results indicate that effects of three factors on explosion hazard are ranked from the most important to the least important as initial pressure, equivalence ratio and ammonia addition. Since ammonia is not conventional fuel, the investigations of $NH_3/H_2/O_2$ mixtures are still limited, especially the deflagration-to-detonation transition in such fuels.

In spite of the above research progress, the safety (e.g. explosion or deflagration-to-detonation transition) of ammonia as a fuel and its blends, e.g. with hydrogen and methane, has not been well understood, which is actually one of the most important aspects when they are widely used in engineering propulsion systems. Typically, the fuel safety characteristics (e.g. flame propagation and explosion) can be tested and therefore understood through the smooth and obstructed channels, in which the locally ignited pre-mixture may develop and finally be detonoted. This process corresponds to Deflagration-to-Detonation Transition (DDT). The DDT has been investigated by numerous researchers due to its practical significance in our daily life and engineering application [25,26]. Channels with obstacles are often used to study flame acceleration and DDT in a controlled manner and has become a model configuration for evaluation of the fuel safety since the presence of obstacles along the channel walls results in faster flame acceleration and drastically shortens the run-up distance [25–27].

High-fidelity numerical simulations of DDT become increasingly popular, since the experimental DDT studies are expensive and also dangerous, due to strict equipment requirements, e.g. high pressure containers, high accuracy sensors, data acquisition systems etc. [28]. Oran and her co-workers have performed a series of DDT simulations in obstructed channels filled with hydrogen-air mixture. They investigated the effects of numerical resolution, ignition mode and channel width in two- and three-dimensional reactive Navier-Stokes simulations using stoichiometric hydrogen-air mixture and a global Arrhenius-type mechanism [29]. Furthermore, they also performed the computations for channels with symmetric and staggered obstacles to explore the effects of obstacle spacing [30]. Their studies show that the flames enhance the strength of shocks which sweep through a turbulent flame brush and generate new shocks. In turn, the shock wave interacts with the flames, thereby creating and driving the turbulence in reacting flow field. The DDT is triggered when the favorable conditions arise in nearby unreacted material through localized ignition centers, or "hot spots". A detonation wavelet can be generated through the Zel'dovich mechanism due to the gradients of local reactivity (e.g. temperature or species concentration) [31]. Most of the above investigations are focused on the hydrogen and simple hydrocarbon (e.g. methane), and very limited work has been done for DDT characteristics of ammonia and its blends.

Liberman and Ivanov adopted two-dimensional DDT simulations of hydrogen-oxygen and ethylene-oxygen mixtures with detailed chemical mechanisms in simulations of DDT in hydrogen-air mixture [27,32]. It is found that their results are different from the phenomena predicted with single-step mechanism and the detonation waves are initiated from the

Please cite this article as: Zhu R et al., Numerical simulation of flame acceleration and deflagration-to-detonation transition in ammonia-hydrogen–oxygen mixtures, International Journal of Hydrogen Energy, https://doi.org/10.1016/j.ijhydene.2020.09.227

fast travelling flame brush [27,32]. The possible reasons were given by Dounia et al. that the multi-step chemical mechanism is far more restrictive than the single-step mechanism regarding the conditions for a hot spot to trigger a detonation in hydrogen-air mixtures [33]. Based on the above work with detailed chemistry, there exist two mechanisms of detonation initiation in DDT, depending on the role of shock waves. The first one is direct detonation initiation triggered at the collision spot by focusing shocks at the flame front, whereas the second is focusing of relatively weak shocks leading to a delayed transition to detonation through the reactivity-gradient mechanism [34].

The objective of this work is to numerically investigate the flame acceleration and DDT of ammonia/hydrogen/oxygen mixtures in a two-dimensional obstructed channel. The Navier-Stokes equations will be solved with detailed chemistry for ammonia and hydrogen oxidation. The rest of this paper is organized as below: the mathematical model and numerical method will be introduced in Section Mathematical model and numerical method. The simulation results and discussion will be presented in Section Results and discussion. The conclusions will be drawn in Section Conclusion.

Mathematical model and numerical method

Governing equation

Two-dimensional fully compressible Navier-Stokes equations (i.e. continuity, momentum, energy and species mass fraction) coupled with the equation of state for calorically perfect gas are solved in this work. Their corresponding equations respectively read [35].

$$\frac{\partial \rho}{\partial t} + \nabla \cdot (\rho \boldsymbol{U}) = 0, \tag{1}$$

$$\frac{\partial (\rho \boldsymbol{U})}{\partial t} + \nabla \cdot (\rho \boldsymbol{U}\boldsymbol{U}) = \nabla \tau - \nabla p, \tag{2}$$

$$\frac{\partial (\rho E)}{\partial t} + \nabla \cdot [(\rho E + p)\boldsymbol{U}] = \nabla \cdot (\boldsymbol{U} \cdot \tau) + \nabla \cdot (k \nabla T) + \dot{\omega}_T, \tag{3}$$

$$\frac{\partial (\rho Y_i)}{\partial t} + \nabla \cdot (\rho Y_i \boldsymbol{U}) = \nabla \cdot (\rho D \nabla Y_i) + \dot{\omega}_i, (i = 1, \ldots, N), \tag{4}$$

$$p = \frac{\rho R T}{M}, \tag{5}$$

where t is time, ρ is the density, $\boldsymbol{U}$ is the velocity vector, p is the pressure, E ($\equiv e + (\boldsymbol{U} \cdot \boldsymbol{U})/2$) is the specific total energy with e being the internal energy. T is the gas temperature, $\dot{\omega}_i$ is the chemical reaction rate of i-th species predicted using Arrhenius formulation, $\dot{\omega}_T$ is the heat release rate from the chemical reactions and k is the thermal conductivity. Y_i is the mass fraction of i-th species, N is the number of chemical species, and D is the mass diffusivity. In the equation of state, i.e. Eq. (5), M is the molecular weight of the mixture, and R is the universal gas constant. The viscous stress tensor τ in Eq. (2) takes the following form

$$\tau = \mu \left[(\nabla \boldsymbol{U}) - (\nabla \boldsymbol{U})^T - \frac{2}{3} (\nabla \cdot \boldsymbol{U}) \boldsymbol{I} \right], \tag{6}$$

where μ is the dynamic viscosity, and is estimated using Sutherland's law. In Eq. (6), $\boldsymbol{I}$ is the unit tensor, and the superscript "T" denotes matrix transposition. Note that the external body force (e.g. gravity) is not taken into consideration here.

Numerical solver and numerical discretization

The equations presented in Section Governing equation are solved using a density-based, multi-component and reactive solver, *RYrhoCentralFoam*, which is developed based on a fully compressible flow solver, *rhoCentralFoam*, in the open source CFD toolbox OpenFOAM 5.0 [36,37]. It uses the semi-discrete, non-staggered central schemes for co-located variables on a mesh of polyhedral cells that have an arbitrary number of faces. The non-reacting solver *rhoCentralFoam* has been validated by Greenshields et al. [37] using a series of benchmark tests, e.g. one-dimensional shock tube and two-dimensional forward step. Good agreements with the analytical or other simulated results are demonstrated about the accuracies of the numerical schemes and implementations [37]. The reactive solver *RYrhoCentralFoam* is validated with laboratory-scale supersonic hydrogen/air autoigniting flames [38] and model supersonic combustor [39,40], and the statistics of the velocity and/or reactive scalar fields are captured well compared with the corresponding measurements [38–40]. Furthermore, the capacities of *RYrhoCentralFoam* are also confirmed through our recent studies about detonative combustion or rotating detonation problems [41–44]. The overall characteristics of detonative combustion and the transient behaviors of the rotating detonation combustion are accurately predicted. In particular, the localized DDT phenomenon and subsequent detonation wave propagation in rotating detonation engines is successfully predicted using *RYrhoCentralFoam*, which accounts for bifurcations of detonation wave number observed from the experiments (e.g. see Ref. [45]). Therefore, the solver *RYrhoCentralFoam* is expected to be able to capture the different combustion dynamics at various stages, including initial premixed flame propagation, acceleration and transition into detonative combustion, the hot-spot formation and shock-flame interactions [25,26,31].

The finite volume method is used for the spatial discretization of Eqs. (1)–(4). An operator-splitting approach is used to solve momentum and energy equations [37]. Specifically, in the first step, an explicit predictor equation is solved for convection of conserved variables. In the second step, an implicit corrector equation for the diffusion of primitive variables is solved. Moreover, second-order semi-discrete, non-staggered, Godunov-type central-upwind scheme developed by Kurganov, Noelle and Petrova [46] (termed as KNP scheme hereafter) are used in *RYrhoCentralFoam* for the convection terms in momentum and energy equations. This enables the formation of flux interpolations considering its transport in any direction due to the compressible flow and wave propagation and avoid the explicit need for a Riemann solver. It is shown that the KNP scheme is competitive with the other

Please cite this article as: Zhu R et al., Numerical simulation of flame acceleration and deflagration-to-detonation transition in ammonia-hydrogen–oxygen mixtures, International Journal of Hydrogen Energy, https://doi.org/10.1016/j.ijhydene.2020.09.227

numerical schemes, e.g. Roe scheme [37]. Detailed chemistry calculations can be performed with *RYrhoCentralFoam* through Eq. (4), and the convection term is predicted using a TVD scheme to ensure the scalar boundness. The diffusive terms in Eqs. (1)–(4) are split into orthogonal and non-orthogonal part to minimize the non-orthogonality error. The second-order Gauss scheme with linear interpolation is used for the orthogonal part and surface interpolation of variable normal gradients is applied for the non-orthogonal part. Implicit second-order Crank-Nicolson scheme is applied for the time discretization. The maximum Courant number is set to be 0.1, which approximately corresponds to the physical time step of 10^{-9} s.

Physical model

Flame acceleration and transition to detonation in ammonia/hydrogen/oxygen ($NH_3/H_2/O_2$) mixtures in an obstructed channel will be numerically studied in this work. In spite of the recent increased interests in ammonia as a fuel [2,47], there are still limited experimental investigations for the explosion characteristics and other safety issues of ammonia and its blends (e.g. with hydrogen and methane). Therefore, in this work, to investigate the flame evolution and DDT of ammonia/hydrogen/oxygen mixtures, we select the obstructed channel as the target configuration, which was previously studied using hydrogen/air mixtures, for instance, by Oran et al. [29,48] and Heidari and Wen [49] through high-fidelity numerical simulations, as well as Teodorczyk et al. [50] through experimental measurements.

To reduce the computational cost, two-dimensional computational domain is considered, as shown in Fig. 1. The validity of the two-dimensional simulations of DDT has been extensively discussed in the literature, e.g. Refs. [25,29,31,51,52]. In general, their results can correctly unveil the critical flame dynamics and transition to detonation, although some detailed or localized phenomena may not be captured to the greatest extent (e.g. flame wrinkling level and turbulence-flame interactions [25,29,31,51,52]). Furthermore, due to the symmetrical geometry, only lower half of the domain is simulated (see Fig. 1) and therefore the obstacles are only placed on the bottom walls.

The dimensions for the simulated domain follow those used by Oran and her co-workers for DDT of hydrogen/air mixtures [29]. The origin of the coordinate lies at the left-lower corner of the domain, as shown in Fig. 1 x is the streamwise direction, while y is the spanwise direction. The length of the computational domain is $L = 16d = 64$ cm ($d = 4$ cm is the distance between two neighboring obstacles), while the height is $H = d/2 = 2$ cm. Therefore, the blockage ratio BR (defined as the ratio of the obstacle height to channel height) is 0.5. Selection of $BR = 0.5$ can render us the sufficient opportunity to observe the salient features of the different stages from initiation of premixed flames and ultimate detonation propagation [29,49,50,53]. Also, there are 16 identical obstacles (denoted by black rectangles in Fig. 1, sequentially from 1st to 16th obstacles), evenly placed along the whole channel with the inter-obstacle spacing d being 4 cm. The distance between the first obstacle and the left wall is $d/2$. The height and thickness of individual obstacles are $h = d/4 = 1$ cm and $l = d/16 = 0.25$ cm, respectively. The blockage ratio and the obstacle spacing are found to have significant effects on flame development and DDT [29,51,54,55]. Nevertheless, these effects on flame acceleration and DDT in hydrogen/ammonia/oxygen mixtures will not be investigated here.

The computational domain is closed at the left end (assumed to be wall as showed in Fig. 1), while open to the atmosphere at the right end, which is assumed to be non-reflective in our simulations. The dashed boundary in Fig. 1 corresponds to the symmetric plane, to mimic the geometrical symmetry of this channel. In addition, the left end, bottom and the obstacles are all slip and adiabatic walls. In addition, the initial velocity of the premixed gas is assumed to be zero, and the initial temperature and initial pressure in the channel are 300 K (T_0)and 1 atm (p_0), respectively.

This domain is discretized using a hexahedral mesh with uniform cell size both in the x-direction and y-direction. Following the similar method by Oran et al. [29,30], we utilize a quarter-circle hot kernel (see Fig. 1) with temperature of 2000 K with the radius of 2 mm to ignite an outwardly propagating flame in the premixed gas. This hot kernel is sufficient to successfully ignite a deflagrative flame, but would not directly detonate the mixture in the channel.

A detailed chemical mechanism for ammonia/hydrogen/oxygen mixture is used, which has 31 species and 204 elementary reactions [56]. This mechanism is validated with the experimental data under high pressure and temperature conditions by Song et al. [56]. The DDT transients under various initial compositions of the mixture will be studied in this work and is parametrized through the mass ratio β between the NH_3 and O_2 and molar ratio α between the NH_3 and H_2, i.e.

$$\beta = \frac{17\alpha}{24\alpha + 16}. \tag{7}$$

The reaction system we investigate is premixed stoichiometric $NH_3/H_2/O_2$ mixture. Here we define the fuel/oxidizer stoichiometry following the two overall reactions for NH_3 and H_2 as $4NH_3 + 3O_2 \rightarrow 2N_2 + 6H_2O$ and $2H_2 + O_2 \rightarrow 2H_2O$, respectively. The investigated molar ratios of NH_3 to H_2 (α) are gradually decreased as 4:1, 2:1, 1:1, 1:2, 1:3 and 1:7. For comparisons, we also investigate DDT process in the premixed stoichiometric hydrogen/oxygen mixture (i.e. $\alpha = 0$), and the results will also be presented in Section Results and

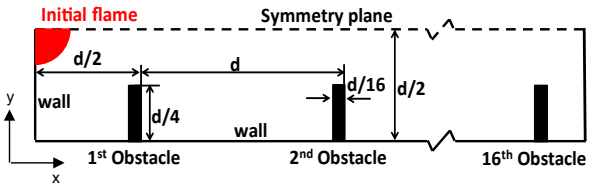

Fig. 1 – Schematic of the computational domain and boundary condition (the spacing between neighboring obstacles is $d = 4$ cm) [29]. The red pocket with high temperature (200 K) is the numerical spark to initiate the flame. (For interpretation of the references to color in this figure legend, the reader is referred to the Web version of this article.)

Please cite this article as: Zhu R et al., Numerical simulation of flame acceleration and deflagration-to-detonation transition in ammonia-hydrogen–oxygen mixtures, International Journal of Hydrogen Energy, https://doi.org/10.1016/j.ijhydene.2020.09.227

discussion. The molar fractions for the cases simulated in the paper are illustrated in Table 1. However, for stoichiometric ammonia/oxygen mixture ($\alpha \rightarrow +\infty$), only NH_3 flame propagation when it is initially ignited can be seen (although the speed is slow, and finally it is quenched) and no DDT phenomenon occurs, and therefore the results will not be presented here.

The ZND structure

The ZND (Zeldovich-Neumann-Döring) structures of ammonia are previously studied by Mevel et al. [57] and Shepherd et al. [58], and their results demonstrate that the detonation relevant quantities (e.g. reaction zone thickness) vary considerably with the initial composition of ammonia-containing mixtures. Therefore, it is conducive to first understand the ZND structures of the investigated $NH_3/H_2/O_2$ mixtures prior to the parametric two-dimensional calculations. The Shock & Detonation Toolbox [59] (abbreviated as "SDToolbox" hereafter) is utilized here to predict the $NH_3/H_2/O_2$ ZND structures. The mechanism from Song et al. [56] is used, and the initial temperature and pressure in these calculations are assumed to be $T_0 = 300$ K and $p_0 = 1$ atm, respectively, in line with the initial conditions for the two-dimensional DDT simulations.

Fig. 2(a) shows the spatial distributions of pressure, temperature and thermicity from the ZND structure when the fuel molar ratio is $\alpha = 2{:}1$. The shock wave lies at $x = 0$. The thermicity σ denotes the heat release resulting from the chemical reactions behind the shock wave [60]. Across the shock wave, the temperature and pressure sharply increase to 1900 K and 45 atm, respectively. Finite heat release from the chemical reactions are found since around $x = 0.05$ mm, characterized by obvious temperature increase in Fig. 2(a). The half width of the heat release pulse (Δ_e) and the distance between the leading shock wave and the peak heat release location(Δ_i) are

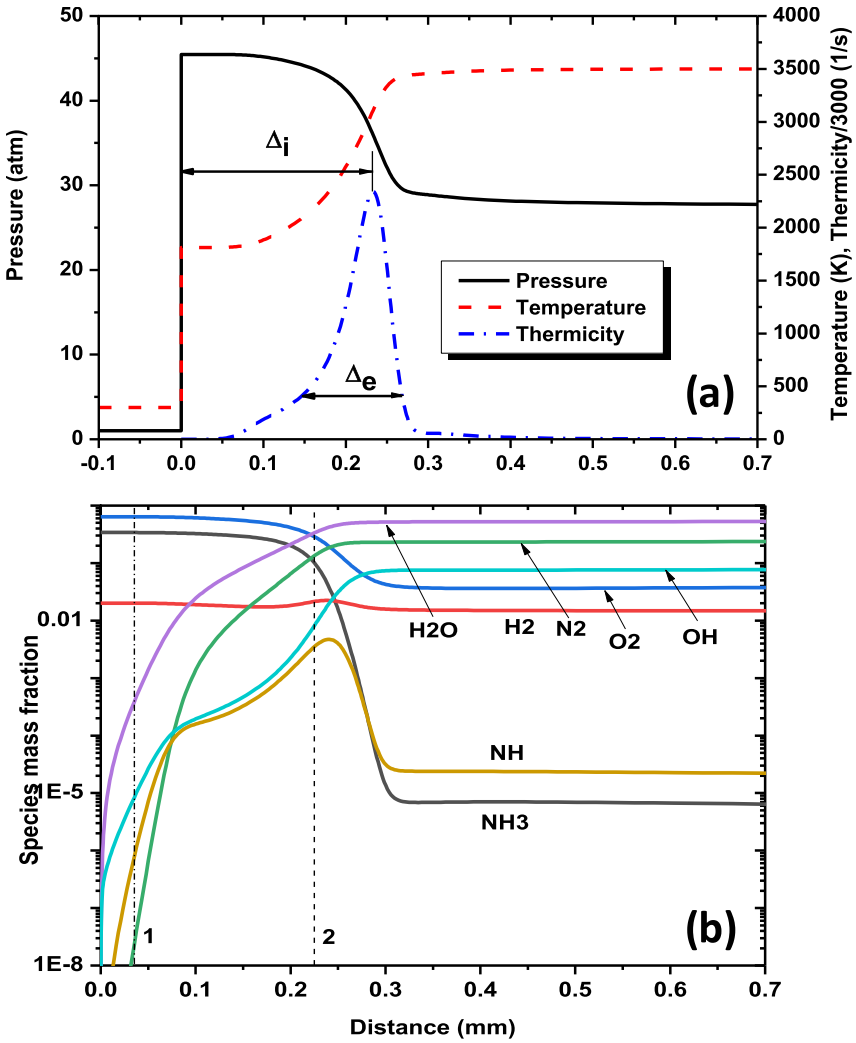

Fig. 2 – Distributions of (a) pressure, temperature, thermicity and (b) key species mass fractions in $NH_3/H_2/O_2$ mixture with fuel molar ratio $\alpha = 2{:}1$. In (a), Δ_e is the half width of the heat release pulse, while Δ_i is the distance between the leading shock wave and maximum heat release location. In (b), Line 1 denotes the location of the shock wave, while Line 2 the location with maximum heat release.

Please cite this article as: Zhu R et al., Numerical simulation of flame acceleration and deflagration-to-detonation transition in ammonia-hydrogen–oxygen mixtures, International Journal of Hydrogen Energy, https://doi.org/10.1016/j.ijhydene.2020.09.227

Table 1 – Molar fractions of ammonia (x_{NH_3}), hydrogen (x_{H_2}) and oxygen (x_{O_2}) for the simulations in various $NH_3/H_2/O_2$ mixtures.

α	x_{NH_3}	x_{H_2}	x_{O_2}
4:1	0.4706	0.1176	0.4118
2:1	0.4000	0.2000	0.4000
1:1	0.3077	0.3077	0.3846
1:2	0.2105	0.4211	0.3684
1:3	0.1600	0.4800	0.3600
1:7	0.0816	0.5714	0.3469
no ammonia	0.0000	0.6667	0.3333

0.059 mm and 0.233 mm, respectively. In the work, the half-reaction length is assumed to be equal to Δ_i in the calculated ZND structure.

Plotted in Fig. 2(b) are the profiles of mass fractions of key species for the same case. Behind the shock wave (Line #1 in Fig. 2(b)), the mass fractions of the reactants NH_3 and O_2 gradually decrease. After Line #2 where maximum heat release occurs, they sharply decrease to relatively low values. For intermediate species, NH increases gradually and has its maximum value at the position of the largest thermicity, and then decrease to a constant value after about $x = 0.3$. Conversely, OH and the product species, N_2 and H_2O, monotonically increases to a constant value after the reaction zone.

For $NH_3/H_2/O_2$ mixtures with other fuel molar ratios α, the respective ZND structures are qualitatively similar to the results in Fig. 2. However, significant differences are still observed among them, in terms of half-reaction length and Chapman–Jouguet (C–J) velocity, which can be clearly observed in Fig. 3. Specifically, with decreased fuel molar ratio α from 4:1 to 1:7, the half-reaction length decreases from 0.375 mm to 0.05 mm, while the C–J velocity increases gradually from 2495 m/s to 2746 m/s. This indicates that when the concentration of hydrogen is increased, the reactivity of the mixture accordingly increases, thereby resulting in shorter ignition delay and induction length.

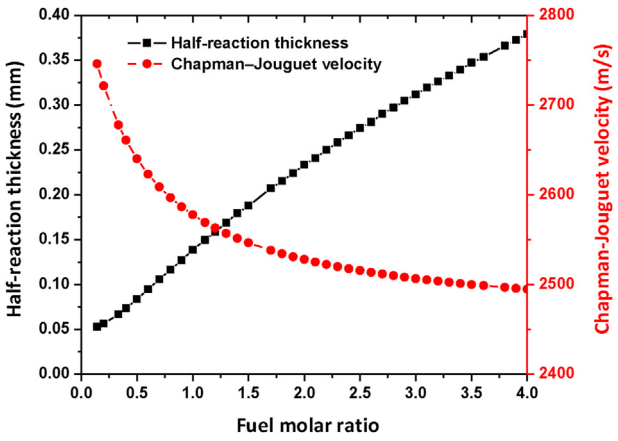

Fig. 3 – Computed half-reaction length and C–J velocity as functions of NH_3/H_2 molar ratio α in stoichiometric $NH_3/H_2/O_2$ mixtures.

Results and discussion

Mesh resolution analysis

In DDT modelling, the influences of the mesh resolution on the global and localized features of flame development should be examined. Therefore, three different static meshes with the uniform cell sizes of 0.2 mm, 0.1 mm, 0.05 mm are chosen to simulate the flame propagation and DDT transients in the $NH_3/H_2/O_2$ mixture. The NH_3/H_2 molar ratio considered here is $\alpha = 2:1$. The above mentioned three cell sizes respectively correspond to about 1, 2, and 4 computational cells per half-reaction length (i.e. 0.2 mm as indicated in (Fig. 3). Fig. 4(a) and (b) and shows the time histories of the locations of reactive front and shock wave front as well as the volume averaged Heat Release Rate (HRR) in the computational domain. The positions of flame front and shock wave are identified as the maximum location in the x direction where the temperature value is over 1800 K and the pressure value is over $1.5p_0$, respectively [29]. Other criteria (e.g. fuel species mass fraction) are also tested, but the effects on the flame location identification are relatively small. The results show that the flame front and the shock wave couple, and therefore the detonation wave is formed at about 0.28 m with the low-resolution (0.2 mm) and the medium-resolution (0.1 mm) meshes, while the onset of detonation is delayed to 0.39 m with the high-resolution (0.05 mm) mesh. The higher resolution can lead to better prediction of the flame front, which would be responsible for larger flame surface area and stronger burning rate and therefore faster propagation of the flame front.

The maximum value of HRR calculated using the high-resolution mesh, more than 1.33×10^{11} J/s, is also larger than the others, 9.51×10^{10} J/s for low-resolution case and 6.51×10^{10} J/s for medium-resolution case. Generally, the results in Fig. 4(a) and (b) and from the three meshes are qualitatively similar. Besides, since only the instantaneous results are discussed here, it is difficult to rule out the stochasticity of the flame characteristics (e.g. flame front instability, hot spot formation and shock structure) caused by the consecutively mesh refinement [29,48,55].

Fig. 5 shows the time sequence of heat release rate (Q_{dot}) fields when a Hot Spot (HS) is formed and then DDT occurs. The results from the three cell sizes are presented for comparisons. It is found that the DDT triggering mechanisms predicted by the three meshes are the same, i.e. due to the generation of a HS at the left corner of the obstacle. However, the HS locations are different as shown in Fig. 5, i.e. it is initiated at the 10^{th} obstacle for the high-resolution mesh, whilst at the 7^{th} obstacle for the low- and medium-resolution meshes. This is consistent with the results presented in Fig. 4. This may be caused by the different computed flame behaviors in high-vorticity areas, such as obstacle wakes. The higher the numerical resolution, the more detailed structures we can resolve and therefore the flame would propagate faster due to higher burning rate [29]. Since the main characteristics of DDT triggering mechanism are captured by all the three meshes, the grid resolution of 0.1 mm will be used here for the following studies with detailed chemistry.

Please cite this article as: Zhu R et al., Numerical simulation of flame acceleration and deflagration-to-detonation transition in ammonia-hydrogen–oxygen mixtures, International Journal of Hydrogen Energy, https://doi.org/10.1016/j.ijhydene.2020.09.227

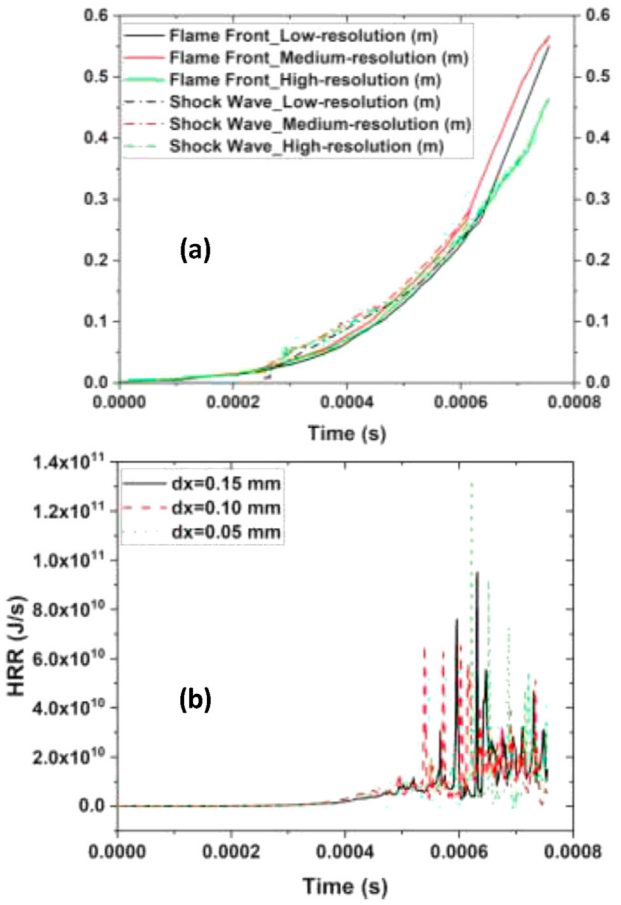

Fig. 4 – Time histories of (a) flame front and shock wave locations and (b) heat release rate computed with three different meshes.

Initial composition effects

Intermediate hydrogen concentration (α = 2:1 and 4:1)

Fig. 6 shows the time sequences of temperature distributions in the DDT process and the fuel molar ratio in the premixed gas is α = 2:1. Each frame shows a 16-cm-long (in x-direction) section of the computational domain, which visualizes the instantaneous locations of the leading reaction front as well as shock (or compression) wave. At t = 0 s (as shown in Fig. 6(a)), the hot kernel with temperature of 2000 K is placed at the left top corner of the domain, which results in the successful initiation and subsequent expansion of the flame front (see Fig. 6(b)). As demonstrated in Fig. 6(c)-(d), considerable wrinkling can be seen along the flame front. This is caused by the front instability due to various mechanisms, e.g. Rayleigh–Taylor (R–T), Richtmyer–Meshkov (R–M) and Kelvin–Helmholtz (K–H) instabilities [26,31]. These unstable fronts can further facilitate the heat release from the premixed flames due to the increased flame surface length. Meanwhile, the shock wave compresses the fresh $NH_3/H_2/O_2$ mixture some distance ahead of the reactive front. As presented in Fig. 7(a), the compressed unreacted mixture ahead of the flame front becomes locally sonic just past the secondobstacle at t = 0.0004 s. Noticeable shocks start to appear just past the third obstacle at t = 0.00045 s, and the supersonic flow region is further expanded before the flame front (see Fig. 7(c)). The average flame velocity gradually increases, and the instantaneous speed arrives at 1500 m/s when t = 0.0007 s (see Fig. 8(c)).

At t = 0.000603 s in Fig. 6(h), a hot spot with temperature over 3000 K appears at the left bottom of the seventh obstacle in the shocked but unreacted premixed gas, and expansion of this kernel is observed from Fig. 6(i). This can be attributed to the compression of premixed gas resulting from the collisions between the Mach stem and the obstacle and is also observed

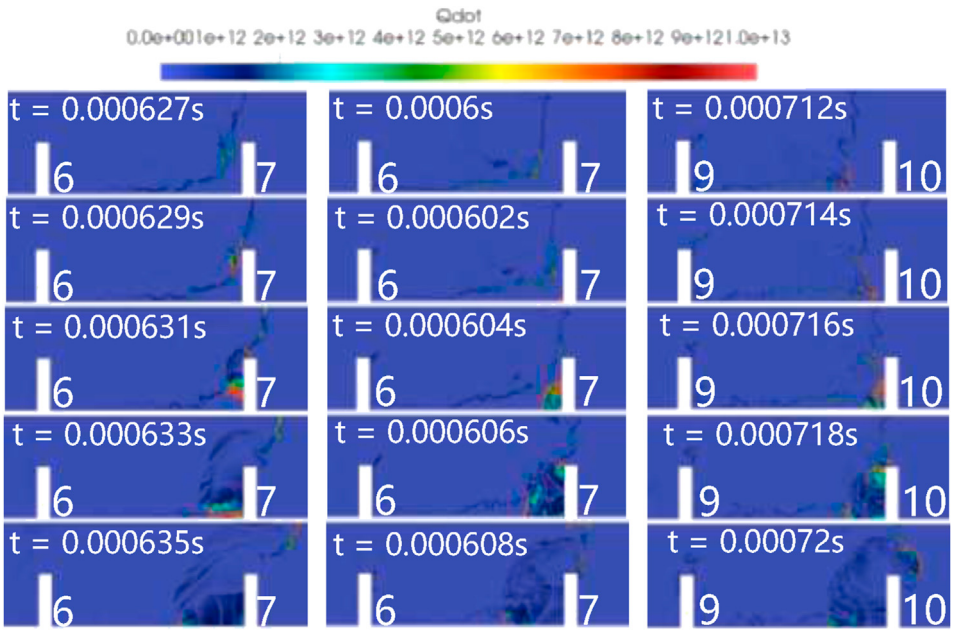

Fig. 5 – Time sequence of heat release rate distributions when DDT occurs predicted with different grid sizes 0.15, 0.1 and 0.05 mm (from left to right).

Please cite this article as: Zhu R et al., Numerical simulation of flame acceleration and deflagration-to-detonation transition in ammonia-hydrogen–oxygen mixtures, International Journal of Hydrogen Energy, https://doi.org/10.1016/j.ijhydene.2020.09.227

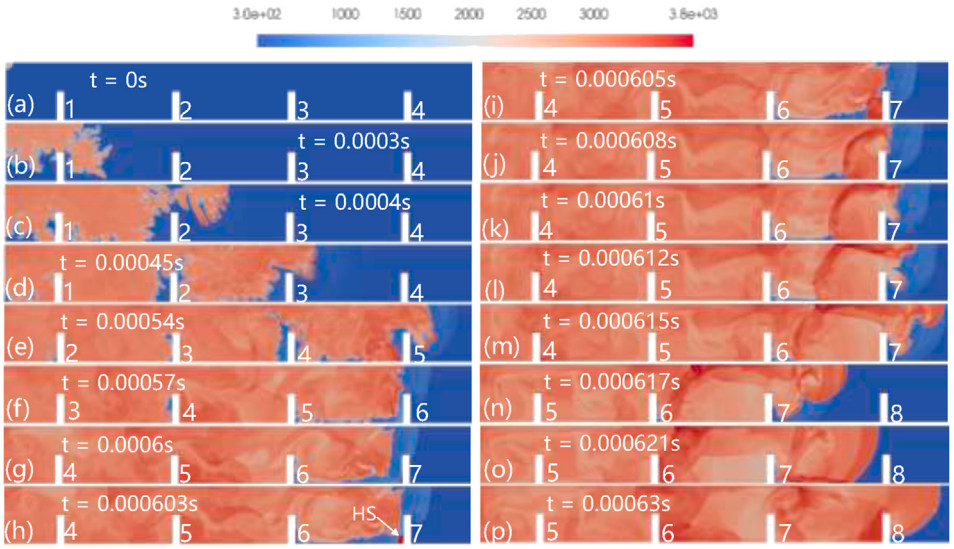

Fig. 6 – Time sequence of temperature (in Kelvin) distributions for the stoichiometric $NH_3/H_2/O_2$ mixture with NH_3/H_2 molar ratio $\alpha = 2{:}1$. The numbers near the obstacles indicate their respective labels. HS denotes the hot spot.

in the DDT processes of other fuels, e.g. H_2/air mixture [29,30] and hydrocarbon/air mixture [51]. The kernel expands, consumes the premixed gas between the seventh obstacle and the approaching flame front (see Fig. 6i and j). Its fast growth leads to both retonation and detonation fronts, and the latter further passes through the narrow gap between the upper and lower obstacles and overtakes the leading reactive front, resulting in a jet of the hot gas close to the symmetry plane into the unburned $NH_3/H_2/O_2$ mixture (as shown in Fig. 6m). This stream quickly catches up with the shock due to the local supersonic gas speed (see the Mach number distributions in Fig. 7d and e), and is finally coupled with it, leading to formation of the detonation front, as presented in Fig. 6(n). The localized detonative front is quickly evolved into a self-sustainable detonation front in the channel and propagates towards the exit of the domain, although frequent diffraction occurs after passing the rest of the obstacles. This similar mechanism for DDT is also observed in Refs. [29,30,51].

Plotted in Fig. 8 is the time sequence of the temperature fields after the flame is ignited when the NH_3/H_2 molar ratio in the stoichiometric mixture is $\alpha = 4{:}1$. Compared to the mixture discussed in Figs. 6 and 7, here the molar concentration of ammonia is doubled. The initial flame development (e.g. $t = 0.00055$ s) is qualitatively similar to what is observed in Fig. 6. Then the flame is gradually accelerated, and the instantaneous speed arrives at 1500 m/s when $t = 0.0007$ s (see Fig. 8(c)). At $t = 0.000817$ s, a hot spot (denoted by HS1 in Fig. 8(f)) with temperature over 3000 K appears at the left bottom of eighth obstacle in the unreacted gas. This phenomenon is similar to that with the fuel molar ratio $\alpha = 2{:}1$ in Fig. 6. Differently, the detonation wave expanded from this explosive point weakens after it passes the obstacle gap, and hence fails to overtake the preceding shock wave. As seen from Fig. 8(h) and (i), the coupling between the reactive front and shock wave does not occur. The similar process also occurs at the left bottom of the ninth obstacle at $t = 0.000849$ s, the tenth one at $t = 0.000885$ s, the eleventh one at $t = 0.000914$ s and fourteenth one at $t = 0.000987$ s, marked as HS2 to HS5 in Fig. 8, respectively. In spite of the frequent generation of the explosive pockets around the corner of the obstacles, the induced reactive front does not become coupled with the leading shock, and transition into detonation combustion is not seen here. The alternate occurrence of the detonation failure and re-ignition is also observed in Refs. [29,30,51]. Therefore, different from the results in Fig. 6,

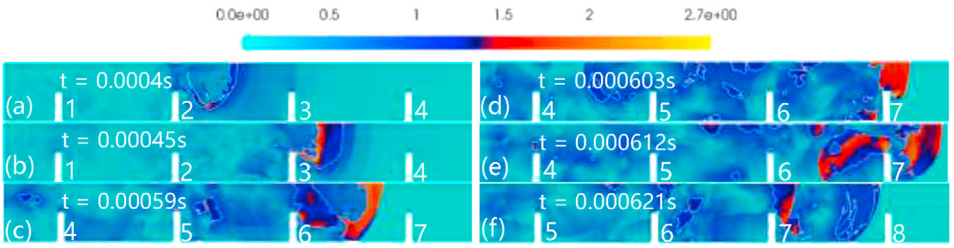

Fig. 7 – Time sequence of local Mach number distributions for the stoichiometric $NH_3/H_2/O_2$ mixture with NH_3/H_2 molar ratio $\alpha = 2{:}1$. The numbers near the obstacles indicate their respective labels. The white iso-lines denote the local sonic conditions.

Please cite this article as: Zhu R et al., Numerical simulation of flame acceleration and deflagration-to-detonation transition in ammonia-hydrogen–oxygen mixtures, International Journal of Hydrogen Energy, https://doi.org/10.1016/j.ijhydene.2020.09.227

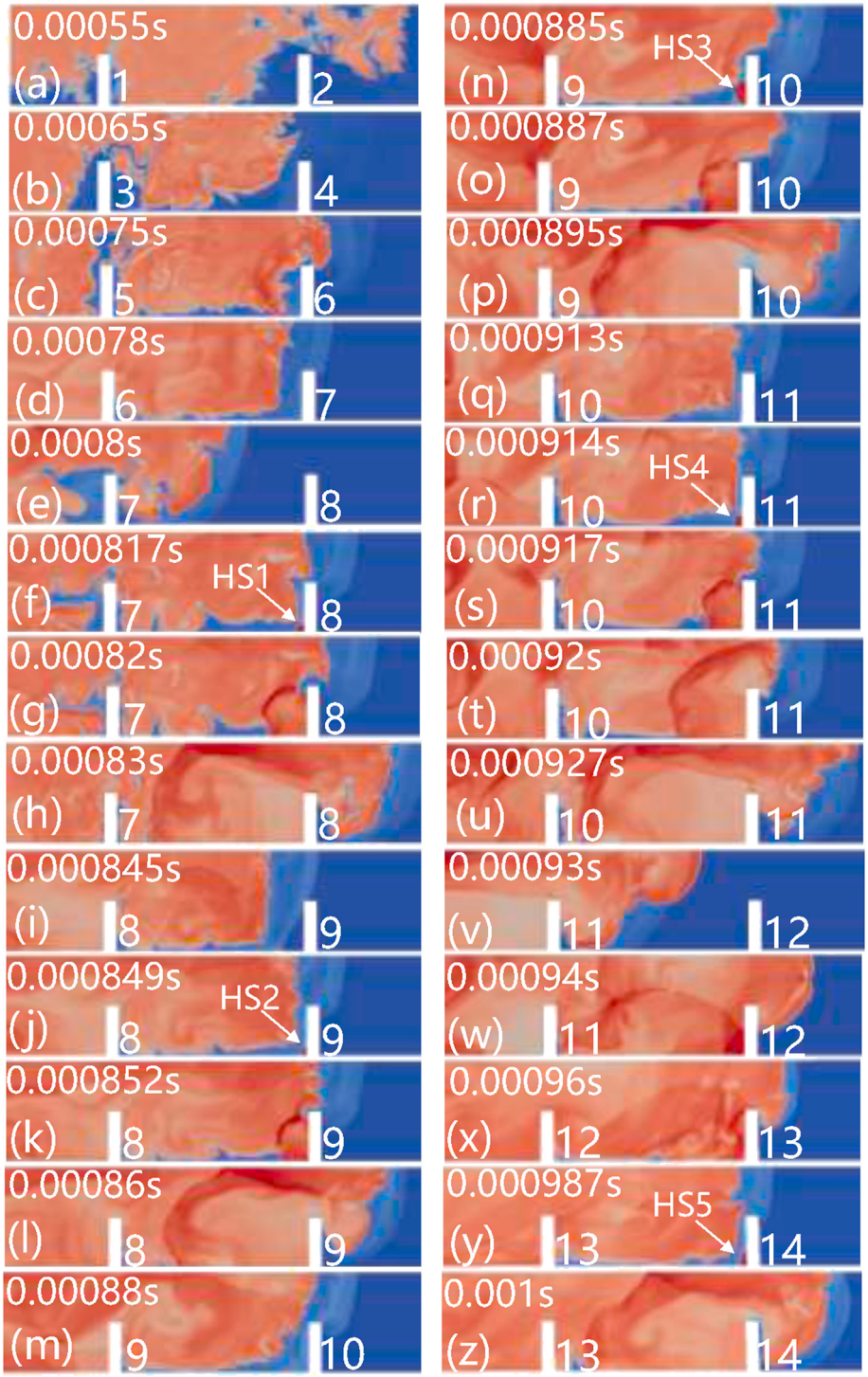

Fig. 8 – Time sequence of temperature (in Kelvin) distributions for stoichiometric $NH_3/H_2/O_2$ mixture with NH_3/H_2 molar ratio $\alpha = 4{:}1$. The numbers near the obstacles indicate their respective labels. HS1-HS4 denote the hot spots.

ultimate development into detonation front propagation is not found in the current mixture with fuel molar ratio $\alpha = 4{:}1$.

High hydrogen concentration (α = 1:1, 1:2, 1:3, 1:7 and 0)

Flame acceleration and DDT processes are simulated using stoichiometric $NH_3/H_2/O_2$ mixture with higher hydrogen concentration, i.e. $\alpha = 1{:}1$, 1:2, 1:3 and 0. Here $\alpha = 0$ indicates no ammonia and pure hydrogen in the mixture. Fig. 9 shows the evolutions of the instantaneous temperature distributions in the mixtures with $\alpha = 1{:}1$ and 1:2, whilst plotted in Fig. 10 are the results from the cases with $\alpha = 1{:}3$, 1:7, and 0. For $\alpha = 1{:}1$, at $t = 0.00035$ s after the flame is initiated, a hot spot is formed at the flame front when it propagates towards the fourth obstacle (see Fig. 9). Then it grows fast in the unreacted gas between the flame front and the neighboring fourth obstacle. Its collision with the fourth obstacle results in strong shock

Please cite this article as: Zhu R et al., Numerical simulation of flame acceleration and deflagration-to-detonation transition in ammonia-hydrogen–oxygen mixtures, International Journal of Hydrogen Energy, https://doi.org/10.1016/j.ijhydene.2020.09.227

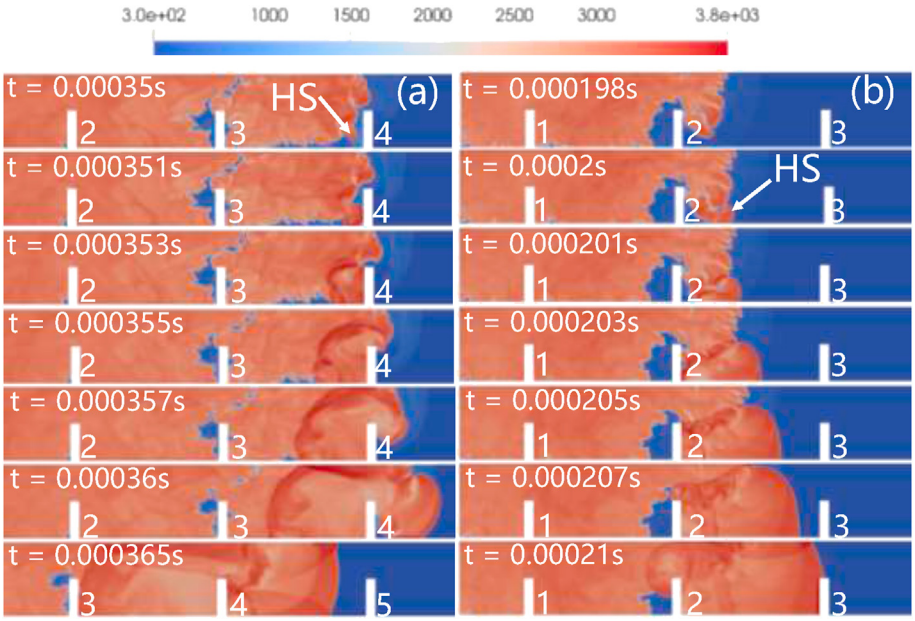

Fig. 9 – Time sequence of temperature (in Kelvin) distributions of the stoichiometric $NH_3/H_2/O_2$ mixture with NH_3/H_2 molar ratio α = (a) 1:1 and (b) 1:2.

waves propagating backward and forward, similar to the subsequent developments of the hot spot observed in Figs. 6 and 8. The detonative front is formed at t = 0.00036 s in Fig. 9(a). Although all the explosive hot spots in Fig. 9(a) and in Figs. 6 and 8 occur when the fast-moving flame front approaches the obstacle, nevertheless, different from the results of the mixtures in α = 2:1 and 4:1, here the hot spot may be caused by the enhancement of the shock waves reflected from the obstacle ahead.

For the stoichiometric $NH_3/H_2/O_2$ mixture with α = 1:2, detonation transition from the deflagrative flames is triggered also from a hot spot along the flame front (see the second frame of Fig. 9(b)). At t = 0.0002 s, an explosive spot is formed at the flame front when it approaches the channel bottom wall surface. This is similar to scenario observed in Fig. 9(a). However, differently, here the interactions between the flame front and channel bottom, instead of the vertical obstacle, dominate. The spot also generates the retonation, diffracting

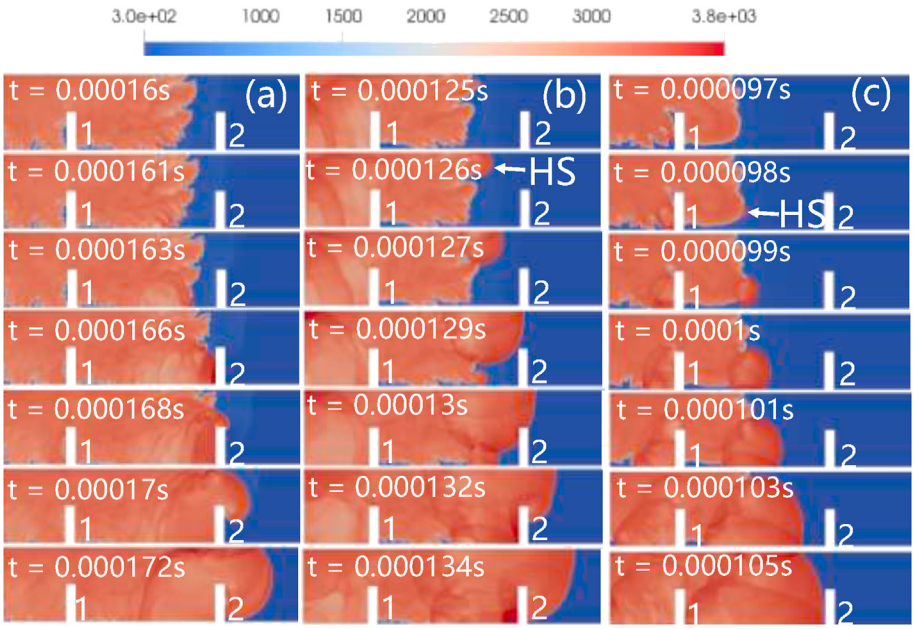

Fig. 10 – Time sequence of temperature (in Kelvin) distributions of the stoichiometric $NH_3/H_2/O_2$ mixture with NH_3/H_2 molar ratio α = (a) 1:3, (b) 1:7 and (c) no ammonia.

Please cite this article as: Zhu R et al., Numerical simulation of flame acceleration and deflagration-to-detonation transition in ammonia-hydrogen–oxygen mixtures, International Journal of Hydrogen Energy, https://doi.org/10.1016/j.ijhydene.2020.09.227

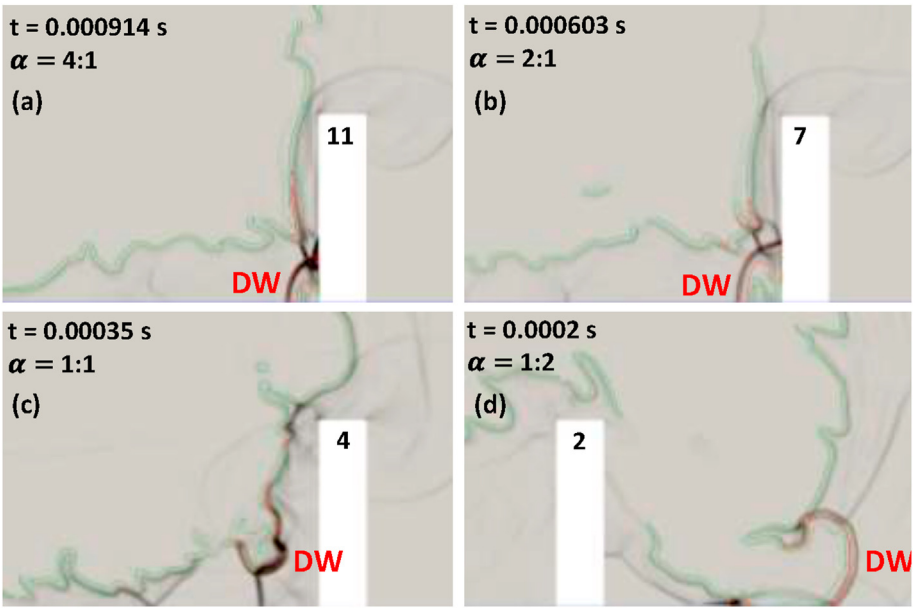

Fig. 11 – Distributions of density gradient (in kg/m^4) for α = (a) 4:1, (b) 2:1, (c) 1:1 and (d) 1:2. The green and red isolines denote the heat release rates of 10^{12} J/m^3/s and 10^{13} J/m^3/s, respectively. DW denotes the newly ignited detonation wave. (For interpretation of the references to color in this figure legend, the reader is referred to the Web version of this article.)

through the second obstacle and depleting the residual unburned mixture at the corner (see the last frame of Fig. 9(b)).

Higher hydrogen concentrations are also considered to examine the corresponding DDT characteristics. In Fig. 10(a) with α = 1:3, when the flame front approaches the second obstacle, the strong compression due to the obstacle wall leads to the transition into the detonative combustion, as can be seen in Fig. 10(a). In this case, no salient localized hot spots are observable along the flame front and/or in the shocked but unburned gas before the reactive front. However, when the hydrogen concentration is further increased to, e.g. α = 1:7 in Fig. 10(b) and even 100% hydrogen (α = 1:7) in Fig. 10(c), hot spots always arise from the flame front. In Fig. 10(b), a second hot spot also appears close to the bottom wall when the first is expanding. However, the second one is quickly weakened due to the insufficient fuel.

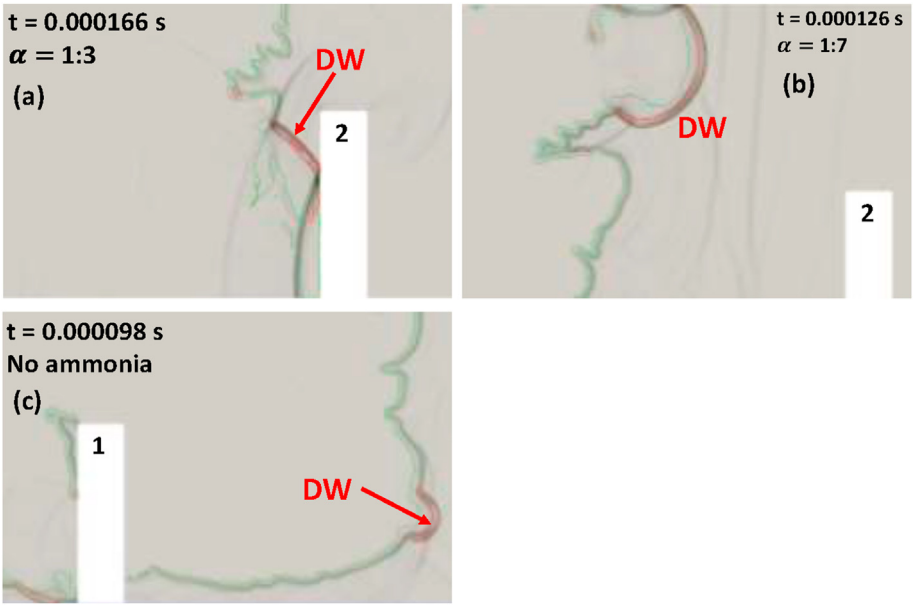

Fig. 12 – Distributions of density gradient (in kg/m^4) for α = (a) 1:3, (b) 1:7, (c) 0. The green and red iso-lines denote the heat release rates of 10^{12} J/m3/s and 10^{13} J/m3/s, respectively. DW denotes the newly ignited detonation wave. (For interpretation of the references to color in this figure legend, the reader is referred to the Web version of this article.)

Please cite this article as: Zhu R et al., Numerical simulation of flame acceleration and deflagration-to-detonation transition in ammonia-hydrogen–oxygen mixtures, International Journal of Hydrogen Energy, https://doi.org/10.1016/j.ijhydene.2020.09.227

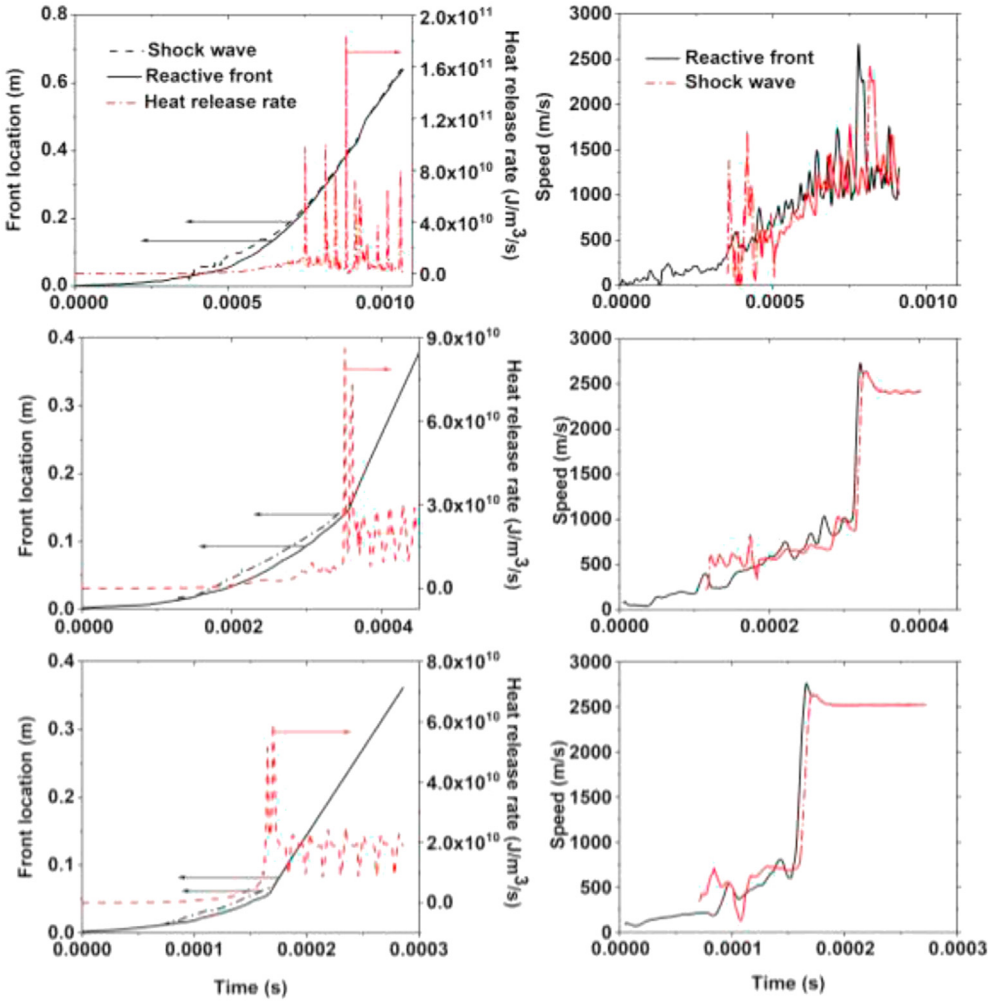

Fig. 13 – Time series of (left column) the front locations, global heat release rate and (right column) the propagation speed of the fronts for different NH_3/H_2 molar ratios: α = 4:1, 1:1 and 1:3 (from first row to third row).

Hot spot formation in various $NH_3/H_2/O_2$ mixtures

Explosive hot spots play a significant role in transition of deflagrative flames into detonation based on the results discussed in section Hot spot formation in various $NH_3/H_2/O_2$ mixtures and Refs. [25,26,31]. They are generated due to enhancement of the reactivity of the unburned mixture or the deflagrative front by shock waves. The two ammonia-dominated cases are in accordance with the Zel'dovich gradient mechanism that detonations appear when local conditions in unreacted material allow a spontaneous reactive wave to form and subsequent become a detonation propagating outside the gradient [31]. While DDT is triggered all when the flame surface goes through a collision with a wall when α = 1:1, 1:2 and 1:3 as shown in Figs. 11 and 12, the time of which are 0.351 ms, 0.2 ms and 0.161 ms, respectively. The mechanism is justified by the fact that a shock wave (visualized by the strong density gradient in Figs. 11 and 12) is reflected from the bottom wall or obstacle surface that cross the flame front, thereby leading to detonation initiation inside the flame brush. In these situations, DDT is triggered by the interactions of a shock with a flame front, and this is also observed by Dounia et al. in DDT simulations with detailed chemistry [33]. Besides, hot spots both form in the two hydrogen-dominant mixtures after the flame fronts pass O_1 at 0.126 ms and 0.098 ms, which are shown in Fig. 12(b) and (c). The underlying possible mechanism is that the reactivity of the local reactants is sufficiently high to produce a pocket of heated and compressed gas adjacent to the flame front due to the compression effects of the neighboring obstacles.

Evolutions of front location and heat release rate

Fig. 13 presents the time histories of the location and propagation speed of the shock wave and reactive front as well as the global heat release rate when the fuel molar ratios are α = 4:1, 1:1 and 1:3. Here the global heat release rate is obtained through integrating the heat release rate in the entire computational domain, and the phenomenon is observed that as the concentration of ammonia decreases, the acceleration of flame, the appearance of noticeable shocks and the detonation ignition are all advanced accordingly. Shocks appear at

Please cite this article as: Zhu R et al., Numerical simulation of flame acceleration and deflagration-to-detonation transition in ammonia-hydrogen–oxygen mixtures, International Journal of Hydrogen Energy, https://doi.org/10.1016/j.ijhydene.2020.09.227

0.369 ms, 0.127 ms and 0.071 ms and sudden acceleration of the flame occurs around 0.79 ms, 0.33 ms and 0.15 ms, respectively. Exothermic speed peaks and the shock and flame positions merge when DDT occurs, and the run-up distances are 0.42 m, 0.14 m and 0.06 m, in keeping with the corner of O_{11}, O_4 and O_2. Compared to the cases with low ammonia molar concentrations, consistent fluctuations of the flame and shock speeds are identified when $\alpha = 4{:}1$. The obstructed channel keeps shrinking and expanding like a piston, the flame propagation speed also goes up and down, while the compression effect leads to overall acceleration. The repetitive detonation onset and decoupling when $\alpha = 4{:}1$ intensify the diffraction phenomenon caused by obstacles and trigger more complex flame and shock interactions.

The detonation wave propagation velocities for $\alpha = 1{:}1$ and 1:3 are about 2400 m/s and 2500 m/s, respectively, slightly below the corresponding C-J speeds due to the influence of obstacle blockage. The detonation waves once DDT occurs run more slowly in the mixture with high ammonia molar concentration. High concentration of ammonia in the initial mixture give rise to the ignition-decoupling-re-ignition appearance, during which the propagation velocities of flame and leading shock strongly fluctuate.

Conclusions

Characteristics of flame propagation and DDT in a two-dimensional obstructed channel filled with stoichiometric ammonia-hydrogen-oxygen mixtures are numerically investigated in this work. The fully compressible Navier-Stokes equations coupled with the calorically perfect gas equation are solved and a detailed chemical mechanism is used.

For premixed gas with the ammonia-hydrogen molar ratio $\alpha = 4{:}1$ and 2:1, the flame front interacts with the obstacles and becomes convoluted, and then both the flame surface area and the heat release rate increase. Then at later stages, as the flame front and the shock waves accelerate, and the obstacles diffract and reflect the shock waves. A localized hot spot with temperature appears in the unreacted material, and then DDT is triggered by the Zel'dovich mechanism when a gradient of reactivity forms inside a pocket of unreacted material for $\alpha = 2{:}1$. However, for $\alpha = 4{:}1$, detonation initiation and failure alternatively occurs and therefore no stable propagation of detonation waves is observed.

For $\alpha = 1{:}1$, 1:2, 1:3, 1:7 and no ammonia case, the DDT is triggered when the flame front interacts with the reflected shock waves from either the bottom wall or the obstacle in the channel. This is different from DDT triggering process for foregoing higher molar ratio. Furthermore, as the molar concentration of the ammonia decreases, the flame acceleration, the appearance of noticeable shocks and the deflagration-to-detonation transition occur earlier, and the ultimate detonation wave propagation velocities increase accordingly.

The flame cannot propagate in premixed ammonia-oxygen mixture (no hydrogen) using our current ignition mode. However, when the hydrogen concentration is further increased to 100% (no ammonia), the hot spot arises from the flame front and detonation can be easily ignited. The hydrogen-ammonia blends detonation could overcome some drawbacks of detonation in pure hydrogen and pure ammonia fuel, and its practical applications deserve further investigation.

Declaration of competing interest

The authors declare that they have no known competing financial interests or personal relationships that could have appeared to influence the work reported in this paper.

Acknowledgements

The numerical simulations were performed with the computational resources from National Supercomputing Center, Singapore (NSCC, https://www.nscc.sg/). The suport from Singapore Ministry of Education Tier 1 Grant (R-265-000-688-114) is acknowledged.

REFERENCES

[1] Kojima Y. A green ammonia economy economy. In: 10th annu NH3 fuel conf; 2013.
[2] Kobayashi H, Hayakawa A, Somarathne KDKA, Okafor EC. Science and technology of ammonia combustion. Proc Combust Inst 2019;37:109–33.
[3] Gao Y, Zhang B, Ng HD, Lee JHS. An experimental investigation of detonation limits in hydrogen–oxygen–argon mixtures. Int J Hydrogen Energy 2016;41:6076–83.
[4] Hu E, Huang Z, Liu B, Zheng J, Gu X. Experimental study on combustion characteristics of a spark-ignition engine fueled with natural gas–hydrogen blends combining with EGR. Int J Hydrogen Energy 2009;34:1035–44.
[5] Hu E, Huang Z, Liu B, Zheng J, Gu X, Huang B. Experimental investigation on performance and emissions of a spark-ignition engine fuelled with natural gas–hydrogen blends combined with EGR. Int J Hydrogen Energy 2009;34:528–39.
[6] Wang J, Huang Z, Tang C, Miao H, Wang X. Numerical study of the effect of hydrogen addition on methane–air mixtures combustion. Int J Hydrogen Energy 2009;34:1084–96.
[7] Deng J, Ma F, Li S, He Y, Wang M, Jiang L, et al. Experimental study on combustion and emission characteristics of a hydrogen-enriched compressed natural gas engine under idling condition. Int J Hydrogen Energy 2011;36:13150–7.
[8] Akansu S, Kahraman Ceper B. Experimental study on a spark ignition engine fuelled by methane–hydrogen mixtures. Int J Hydrogen Energy 2007;32:4279–84.
[9] Miao J, Leung CW, Cheung CS. Effect of hydrogen percentage and air jet Reynolds number on fuel lean flame stability of LPG-fired inverse diffusion flame with hydrogen enrichment. Int J Hydrogen Energy 2014;39:602–9.
[10] Tseng C. Effects of hydrogen addition on methane combustion in a porous medium burner. Int J Hydrogen Energy 2002;27:699–707.
[11] Tang C, Huang Z, Jin C, He J, Wang J, Wang X, et al. Laminar burning velocities and combustion characteristics of propane–hydrogen–air premixed flames. Int J Hydrogen Energy 2008;33:4906–14.

Please cite this article as: Zhu R et al., Numerical simulation of flame acceleration and deflagration-to-detonation transition in ammonia-hydrogen–oxygen mixtures, International Journal of Hydrogen Energy, https://doi.org/10.1016/j.ijhydene.2020.09.227

[12] Wu L, Kobayashi N, Li Z, Huang H. Experimental study on the effects of hydrogen addition on the emission and heat transfer characteristics of laminar methane diffusion flames with oxygen-enriched air. Int J Hydrogen Energy 2016;41:2023–36.
[13] Lee JHS. The detonation phenomenon. Cambridge: Cambridge University Press; 2008.
[14] Lee JHS. Dynamic parameters of gaseous detonations. Annu Rev Fluid Mech 1984;16:311–36.
[15] Zhang B. The influence of wall roughness on detonation limits in hydrogen–oxygen mixture. Combust Flame 2016;169:333–9.
[16] Gordon WE, Mooradian AJ, Harper SA. Limit and spin effects in hydrogen-oxygen detonations. Symp Combust 1958;7:752–9.
[17] Lee JJ, Dupré G, Knystautas R, Lee JH. Doppler interferometry study of unstable detonations. Shock Waves 1995;5:175–81.
[18] Duynslaegher C, Jeanmart H, Vandooren J. Ammonia combustion at elevated pressure and temperature conditions. Fuel 2010;89:3540–5.
[19] Valera-Medina A, Marsh R, Runyon J, Pugh D, Beasley P, Hughes T, et al. Ammonia–methane combustion in tangential swirl burners for gas turbine power generation. Appl Energy 2017;185:1362–71.
[20] Frigo S, Gentili R. Analysis of the behaviour of a 4-stroke Si engine fuelled with ammonia and hydrogen. Int J Hydrogen Energy 2013;38:1607–15.
[21] Valera-Medina A, Pugh DG, Marsh P, Bulat G, Bowen P. Preliminary study on lean premixed combustion of ammonia-hydrogen for swirling gas turbine combustors. Int J Hydrogen Energy 2017;42:24495–503.
[22] Hayakawa A, Goto T, Mimoto R, Arakawa Y, Kudo T, Kobayashi H. Laminar burning velocity and Markstein length of ammonia/air premixed flames at various pressures. Fuel 2015;159:98–106.
[23] Lee JH, Lee SI, Kwon OC. Effects of ammonia substitution on hydrogen/air flame propagation and emissions. Int J Hydrogen Energy 2010;35:11332–41.
[24] Li Y, Bi M, Li B, Zhou Y, Huang L, Gao W. Explosion hazard evaluation of renewable hydrogen/ammonia/air fuels. Energy 2018;159:252–63.
[25] Oran ES. Understanding explosions – from catastrophic accidents to creation of the universe. Proc Combust Inst 2015;35:1–35.
[26] Dorofeev SB. Flame acceleration and explosion safety applications. Proc Combust Inst 2011;33:2161–75.
[27] Ivanov MF, Kiverin AD, Liberman MA. Flame acceleration and DDT of hydrogen–oxygen gaseous mixtures in channels with no-slip walls. Int J Hydrogen Energy 2011;36:7714–27.
[28] Heidari A, Wen JX. Numerical simulation of flame acceleration and deflagration to detonation transition in hydrogen-air mixture. Int J Hydrogen Energy 2014;39:21317–27.
[29] Gamezo VN, Ogawa T, Oran ES. Numerical simulations of flame propagation and DDT in obstructed channels filled with hydrogen–air mixture. Proc Combust Inst 2007;31:2463–71.
[30] Gamezo VN, Ogawa T, Oran ES. Flame acceleration and DDT in channels with obstacles: effect of obstacle spacing. Combust Flame 2008;155:302–15.
[31] Oran ES, Gamezo VN. Origins of the deflagration-to-detonation transition in gas-phase combustion. Combust Flame 2007;148:4–47.
[32] Liberman MA, Ivanov MF, Kiverin AD, Kuznetsov MS, Chukalovsky AA, Rakhimova TV. Deflagration-to-detonation transition in highly reactive combustible mixtures. Acta Astronaut 2010;67:688–701.
[33] Dounia O, Vermorel O, Misdariis A, Poinsot T. Influence of kinetics on DDT simulations. Combust Flame 2019;200:1–14.
[34] Xiao H, Oran ES. Shock focusing and detonation initiation at a flame front. Combust Flame 2019;203:397–406.
[35] Poinsot T, Veynante D. Theoretical and numerical combustion. RT Edwards, Inc.; 2005.
[36] Weller HG, Tabor G, Jasak H, Fureby C. A tensorial approach to computational continuum mechanics using object-oriented techniques. Comput Phys 1998;12:620.
[37] Greenshields CJ, Weller HG, Gasparini L, Reese JM. Implementation of semi-discrete, non-staggered central schemes in a colocated, polyhedral, finite volume framework, for high-speed viscous flows. Int J Numer Methods Fluid 2010;63:1–21.
[38] Zhao M, Chen Z, Zhang H, Swaminathan N. Large eddy simulation of A supersonic lifted hydrogen-air flame with perfectly stirred reactor model. 2019.
[39] Huang Z, Zhang H. Numerical investigations of mixed supersonic and subsonic combustion modes in a model combustor. Int J Hydrogen Energy 2020;45:1045–60.
[40] Huang Z, Cleary M, Zhang H. Large eddy simulation of A model supersonic combustor with A sparse-Lagrangian multiple mapping conditioning approach. 2019.
[41] Zhao M, Li J-M, Teo CJ, Khoo BC, Zhang H. Effects of variable total pressures on instability and extinction of rotating detonation combustion. Flow. Turbul Combust 2020;104:261–90.
[42] Zhao M, Zhang H. Modelling rotating detonative combustion fueled by partially pre-vaporized n-heptane sprays. 2020.
[43] Zhao M, Zhang H. Origin and chaotic propagation of multiple rotating detonation waves in hydrogen/air mixtures. Fuel 2020;275:117986.
[44] Zhao M, Cleary M, Zhang H. Combustion mode and wave multiplicity in rotating detonative combustion with separate reactant injection. Combust Flame; 2020. Under Revis.
[45] Bykovskii FA, Zhdan SA, Vedernikov EF. Continuous spin detonations. J Propul Power 2006;22:1204–16.
[46] Kurganov A, Noelle S, Petrova G. Semidiscrete central-upwind schemes for hyperbolic conservation laws and Hamilton–Jacobi equations. SIAM J Sci Comput 2001;23:707–40.
[47] Valera-Medina A, Xiao H, Owen-Jones M, David WIF, Bowen PJ. Ammonia for power. Prog Energy Combust Sci 2018;69:63–102.
[48] Kessler DA, Gamezo VN, Oran ES. Simulations of flame acceleration and deflagration-to-detonation transitions in methane–air systems. Combust Flame 2010;157:2063–77.
[49] Heidari A, Wen JX. Flame acceleration and transition from deflagration to detonation in hydrogen explosions. Int J Hydrogen Energy 2014;39:6184–200.
[50] Teodorczyk A, Drobniak P, Dabkowski A. Fast turbulent deflagration and DDT of hydrogen–air mixtures in small obstructed channel. Int J Hydrogen Energy 2009;34:5887–93.
[51] Goodwin GB, Houim RW, Oran ES. Effect of decreasing blockage ratio on DDT in small channels with obstacles. Combust Flame 2016;173:16–26.
[52] Emami S, Mazaheri K, Shamooni A, Mahmoudi Y. LES of flame acceleration and DDT in hydrogen–air mixture using artificially thickened flame approach and detailed chemical kinetics. Int J Hydrogen Energy 2015;40:7395–408.
[53] Johansen C, Ciccarelli G. Modeling the initial flame acceleration in an obstructed channel using large eddy simulation. J Loss Prev Process Ind 2013;26:571–85.
[54] Ugarte OJ, Bychkov V, Sadek J, Valiev D, Akkerman V. Critical role of blockage ratio for flame acceleration in channels with tightly spaced obstacles. Phys Fluids 2016;28:093602.

Please cite this article as: Zhu R et al., Numerical simulation of flame acceleration and deflagration-to-detonation transition in ammonia-hydrogen–oxygen mixtures, International Journal of Hydrogen Energy, https://doi.org/10.1016/j.ijhydene.2020.09.227

[55] Ogawa T, Oran ES, Gamezo VN. Numerical study on flame acceleration and DDT in an inclined array of cylinders using an AMR technique. Comput Fluids 2013;85:63–70.
[56] Song Y, Hashemi H, Christensen JM, Zou C, Marshall P, Glarborg P. Ammonia oxidation at high pressure and intermediate temperatures. Fuel 2016;181:358–65.
[57] Mével R, Melguizo-Gavilanes J, Chaumeix N. Detonation in ammonia-based mixtures. 11th asia-pacific conf. Combust. ASPACC 2017 2017.
[58] Akbar R, Kaneshige M, Schultz E, Shepherd J. Detonations in H_2-N_2O-CH_4-NH_3-O_2-N_2 mixtures. 2000.
[59] Joe Shepherd. Shock and detonation toolbox. Https://ShepherdCaltechEdu/EDL/PublicResources/Sdt [n.d].
[60] Shepherd JE. Detonation in gases. Proc Combust Inst 2009;32:83–98.

Please cite this article as: Zhu R et al., Numerical simulation of flame acceleration and deflagration-to-detonation transition in ammonia-hydrogen–oxygen mixtures, International Journal of Hydrogen Energy, https://doi.org/10.1016/j.ijhydene.2020.09.227